# Structure and Spectroscopic and Magnetic Properties of Rare Earth Metal(III) Derivatives with the 2-Formyl-4-methyl-6-(*N*-(2-pyridylethyl)formimidoyl)phenol Ligand

**Marius Andruh,[†] Evangelos Bakalbassis,[†] Olivier Kahn,*[,†] Jean Christian Trombe,[‡] and Pierre Porcher[§]**

Laboratoire de Chimie Inorganique, URA No. 420, Université de Paris Sud, 91405 Orsay, France, CEMES-LOE, UPR No. 8011, P.O. Box 4347, 31055 Toulouse, France, and Laboratoire des Eléments de Transition dans les Solides, UPR No. 210, 1 Place Aristide Briand, 92195 Meudon, France

*Received June 22, 1992*

The compounds $[ML_2(H_2O)_4](ClO_4)_3 \cdot 4H_2O$ ((**1**)M), where M is a trivalent rare earth metal and L the bidentate liquid 2-formyl-4-methyl-6-(*N*-(2-pyridylethyl)formimidoyl)phenol, have been synthesized. Single crystals of $[GdL_2(H_2O)_4](ClO_4)_2Cl \cdot 2.75H_2O$ have been obtained, and its crystal structure has been solved. This compound crystallizes in the monoclinic system, space group $P2_1/c$. The lattice parameters are $a = 18.079(4)$ Å, $b = 14.560(3)$ Å, $c = 16.409(3)$ Å, $\beta = 92.93(2)°$, and $Z = 4$. The structure consists of $[GdL_2(H_2O)_4]^{3+}$ cations, perchlorate and chloride anions and noncoordinated water molecules. The Gd atom is surrounded by eight oxygen atoms, four belonging to water molecules and the other four to the carbonyl and phenolic functions of two L ligands. The coordination sphere of Gd is very close to a perfect square antiprism. (**1**) Eu exhibits a strong luminescence in the solid state. The transition energies of the luminescence spectrum have been determined. The temperature dependences of the molar magnetic susceptibility $\chi_M$ for (**1**)M (M = Gd, Nd, Eu, Sm) have been measured. A perfect Curie law is observed for (**1**)Gd. The EPR spectrum reveals a zero-field splitting within the $^8S_{7/2}$ ground state characterized by an axial parameter $|D| = 4.0 \times 10^{-2}$ cm$^{-1}$. $\chi_M T$ for (**1**)Nd decreases from 1.64 cm$^3$ K mol$^{-1}$ at 300 K down to 0.8 cm$^3$ K mol$^{-1}$ at 4.2 K as the temperature T is lowered, due to the crystal-field splitting of the $^4I_{9/2}$ free-ion state. For both (**1**)Eu and (**1**)Sm compound, the first free-ion excited states are thermally populated at 300 K; hence, their magnetic behaviors significantly deviate from the Curie law. The magnetic data have been satisfactorily interpreted in the free-ion approximation. For (**1**)Eu, an excellent agreement between optical and magnetic properties has been obtained.

## Introduction

Three years ago, we initiated a new project concerning rare earth metal molecular chemistry.[1,2] The reasons for that were as follows. (i) From a synthetic point of view, the rare earth metal chemistry is much less developed than the transition metal chemistry. (ii) The high coordination of the rare earth metals may lead to quite unusual molecular structures.[1-13] (iii) The very strong oxophilic character of the trivalent rare earth metals may be used to protect oxygen-containing functions. This allows for the synthesis of molecules that otherwise could not be easily obtained.[2] (iv) The magnetic properties of the rare earth metal compounds, even of the mononuclear species, are still badly understood. In contrast with what happens for transition metal compounds, the angular momentum in general plays a key role. The effect of the crystal field is not easily taken into account without performing very tedious calculations in which the chemical intuition tends to vanish. In 1976, Casey and Mitra wrote a review chapter on the magnetic properties of lanthanide compounds.[14] It is quite striking that in the section concerning selected experimental data only references before 1950 were quoted. Similarly, Carlin devoted a chapter to rare earths in his book written in 1986.[15] This chapter does not discuss the magnetic properties of rare earth metal molecular compounds. (v) If the optical properties of extended lattices containing rare earth metal ions have been extensively studied, new phenomena may be expected in molecular chemistry, in particular in compounds containing both 3d and 4f ions. (vi) Finally, in some cases, the rare earth metal molecular compounds might be precursors of interesting new solid phases.

This paper is devoted to mononuclear species of formula $[ML_2(H_2O)_4](ClO_4)_3 \cdot 4H_2O$ ((**1**)M) where L is the bidentate ligand 2-formyl-4-methyl-6-(*N*-(2-pyridylethyl)formimidoyl)phenol:

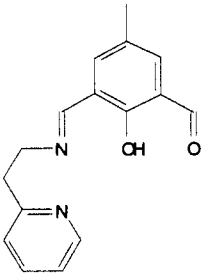


It is worth noting that this ligand had never been reported. We will successively describe the synthesis of the compounds, the

[†] Université de Paris Sud.
[‡] CEMES-LOE.
[§] Laboratoire des Eléments de Transition dans les Solides.

(1) Guillou, O.; Bergerat, P.; Kahn, O.; Bakalbassis, E.; Boubekeur, K.; Batail, P.; Guillot, M. *Inorg. Chem.* **1992**, *31*, 110.
(2) Bakalbassis, E.; Kahn, O.; Sainton, J.; Trombe, J. C.; Galy, J. *J. Chem. Soc., Chem. Commun.* **1991**, 755.
(3) Trombe, J. C.; Gleizes, A.; Galy, J. *C. R. Acad. Sci. Paris Ser. 2* **1982**, *284*, 1369; *Inorg. Chim. Acta* **1984**, *87*, 129.
(4) Petit, J. F.; Trombe, J. C.; Gleizes, A.; Galy, J. *C. R. Acad. Sci. Paris, Ser. 2* **1987**, *304*, 1117.
(5) Gleizes, A.; Maury, F.; Galy, J. *Nouv. J. Chim.* **1984**, *8*, 521.
(6) Frasse, C.; Trombe, J. C.; Gleizes, A.; Galy, J. *C. R. Acad. Sci. Paris, Ser. 2* **1985**, *300*, 403.
(7) Trombe, J. C.; Frasse, C.; Gleizes, A. *C. R. Acad. Sci. Paris, Ser. 2* **1985**, *301*, 483.
(8) Goodgame, D. M. L.; Williams, D. J.; Winpenny, R. E. P. *Polyhedron* 1989, 1531.
(9) Wang, S. *Inorg. Chem.* **1991**, *30*, 2252.
(10) Blake, J.; Milne, P. E. V.; Thornton, P.; Winpenny, R. E. P. *Angew. Chem. Int., Ed. Engl.* **1991**, *30*, 1139.
(11) Benelli, C.; Caneschi, A.; Gatteschi, D.; Pardi, L.; Rey, P. Shum, D. P.; Carlin, R. L. *Inorg. Chem.* **1989**, *28*, 272.
(12) Benelli, C.; Caneschi, A.; Gatteschi, D.; Pardi, L.; Rey, P. *Inorg. Chem.* **1989**, *28*, 275.
(13) Benelli, C.; Caneschi, A.; Gatteschi, D.; Pardi, L.; Rey, P. *Inorg. Chem.* **1990**, *29*, 4223.
(14) Casey, A. T.; Mitra, S. In *Theory and Applications of Molecular Paramagnetism*; Boudreaux, E. A., Mulay, L. N., Eds.; John Wiley: New York, **1976**; p 135 and references therein.
(15) Carlin, R. L. *Magnetochemistry*; Springer-Verlag: Berlin, 1986.

0020-1669/93/1332-1616$04.00/0 

**Table I.** Crystallographic Data for $[GdL_2(H_2O)_4](ClO_4)_2Cl\cdot 2.75H_2O$

| | | | |
|---|---|---|---|
| fw | 1049.83 | $\rho$(calcd), g cm$^{-3}$ | 1.66 |
| space group | $P2_1/c$ | $T$, °C | 21 |
| $a$, Å | 18.079(4) | $\lambda$, Å | 0.710 73 |
| $b$, Å | 14.560(3) | $\mu$(Mo K$\alpha$), cm$^{-1}$ | 18.15 |
| $c$, Å | 16.409(3) | $R^a$ | 0.048 |
| $\beta$, deg | 92.93(2) | $R_w{}^b$ | 0.076 |
| $Z$ | 4 | | |

$^a$ $R = \sum||F_o| - |F_c||/\sum|F_o|$. $^b$ $R_w = \{\sum w(|F_o| - |F_c|)^2/\sum w|F_o|^2\}^{1/2}$ with $w = 1/\sigma_F{}^2$; $\sigma_F = \sigma_I(\mathrm{II}_p)^{-1/2}$; $\sigma_I = [\sigma_c{}^2 + (0.002N_{et})^2]^{1/2}$, where $N_{et}$ is the net count of each reflection.

crystal structure of $[GdL_2(H_2O)_4](ClO_4)_2Cl\cdot 2.5H_2O$, the luminescence properties of (**1**)Eu, and the magnetic properties of the compounds with M = Gd, Nd, Eu, and Sm.

## Experimental Section

**Synthesis. $[GdL_2(H_2O_4](ClO_4)_3\cdot 4H_2O$ ((1)Gd).** To a 1/1 (40 mL) solvent mixture of dry acetonitrile and absolute ethanol containing 2 mmol of 2,6-diformyl-4-methylphenol and 1 mmol of gadolinium(III) perchlorate (purchased from Johnson Matthey) was added dropwise and under continuous stirring 2 mmol of 2-(2-aminoethyl)pyridine dissolved in 20 mL of the same solvent mixture. The resulting yellow solution was stirred for 1 h, and then 10 mL of diethyl ether was slowly added. The mixture was allowed to stand overnight at 4 °C and then was filtered. The precipitate was redissolved in acetonitrile and reprecipitated with diethyl ether. The other (**1**)M (M = Ne, Sm and Eu) compounds were prepared in the same way. X-ray powder spectra indicated that the four (**1**)M compounds are isomorphous. Anal. Calcd for $C_{32}H_{48}N_4O_{24}Cl_3Gd$ ((**1**)Gd): C, 33.82; H, 4.26; N, 4.93; Cl, 9.36; Gd, 13.84. Found: C, 34.25; H, 4.84; N, 4.75; Cl, 9.51; Gd, 13.59. Calcd for $C_{32}H_{48}N_4O_{24}Cl_3Ne$ ((**1**)Ne): C, 34.21; H, 4.31; N, 4.99; Cl, 9.47; Ne, 12.84. Found: C, 34.45; H, 4.64; N, 4.79; Cl, 9.74; Ne, 13.19. Calcd for $C_{32}H_{48}N_4O_{24}Cl_3Sm$ ((**1**)Sm): C, 34.03; H, 4.28; N, 4.96; Cl, 9.42; Sm, 13.31. Found: C, 34.18; H, 4.84; N, 4.45; Cl, 9.48; Sm, 12.98. Calcd. for $C_{32}H_{48}N_4O_{24}Cl_3Eu$ ((**1**)Eu): C, 33.98; H, 4.28; N, 4.95; Cl, 9.40; Eu, 13.44. Found: C, 33.69; H, 4.44; N, 4.61; Cl, 9.31; Eu, 13.19.

Single crystals of $[GdL_2(H_2O)_4](ClO_4)_2Cl\cdot 2.75H_2O$ were obtained as follows: 1 mmol of sodium chloride was added to 1 mmol of (**1**)Gd dissolved in 60 mL of a 1/1 mixture of acetonitrile/ethanol. Pale-yellow prismatic-like single crystals were obtained by slow diffusion of diethylther.

**Crystallographic Data Collection and Structure Determination.** A single crystal of $[GdL_2(H_2O)_4](ClO_4)_2Cl\cdot 2.75H_2O$ was mounted on a CAD4 Enraf-Nonius computer-controlled X-ray diffractometer. Orientation matrices and accurate unit-cell constants were refined by optimizing the setting angles of 25 reflexions with $9.30° < \theta < 17.64°$. Crystallographic data are given in Table I. The standard reflection showed no significant intensity decay. Lorentz–polarization and empirical absorption corrections were applied. Structure determination was carried out using Patterson, Fourier, and difference Fourier syntheses and full-matrix least-squares refinement techniques on a DEC VAX 11-730 computer using programs listed in ref 16. Atomic scattering factors were taken from ref 17. Throughout the refinement the minimized function was $\sum w(F_o - |F_c|)^2$ where $F_o$ and $F_c$ are the observed and calculated structure factor amplitudes. The hydrogen atoms were located from difference Fourier maps and introduced in the last cycles of refinement as fixed contributors. The systematic absence of reflections $0k0$, $k = 2n + 1$ and $h0l$, $l = 2n + 1$, indicated $P2_1/c$ as space group. The reliability factors stabilized at $R = 0.048$ and $R_w = 0.076$ for 333 variables and 5520 reflections with $I > 3\sigma(I)$. In the last cycle the highest variable shift/esd ratio was 0.16 (occurring through the noncoordinated water molecules), and the error in an observation of unit weight was $s = 1.48$. A final difference Fourier synthesis showed only peaks with an electron density of 1 e Å$^{-3}$ (ghost of the gadolinium atom) and less than 0.5 e Å$^{-3}$ for the other atoms. Atomic coordinates and equivalent isotropic displacement parameters are listed in Table II. Selected bond lengths and angles are given in Table III.

(16) Sheldrick, G. M. SHELX, Program for Crystal Structure Determination, University of Cambridge, England, 1976. Johnson C. K. *Ortep, a Fortran Thermal Ellipsoid Plot Program for Crystal Structure Determination*; Report ORNL-3794; Oak Ridge National Laboratory: Oak Ridge, TN 1965.

(17) *International Tables for X-ray Crystallography*; Kynoch Press: Birmingham, England, 1974; Vol. 4, Tables 2.2.A and 2.3.1.

**Table II.** Atomic Coordinates and Equivalent Isotropic Displacement Parameters for the Non-Hydrogen Atoms in $[GdL_2(H_2O)_4](ClO_4)_2Cl\cdot 2.75H_2O$

| atom | $x$ | $y$ | $z$ | $B$,$^a$ Å$^2$ | site occupancy |
|---|---|---|---|---|---|
| Gd | 0.75581(2) | 0.56320(2) | 0.51054(2) | 3.025(8) | |
| OW1 | 0.8765(3) | 0.6031(4) | 0.5631(4) | 5.0(1) | |
| OW2 | 0.7928(3) | 0.7034(4) | 0.4437(3) | 4.4(1) | |
| OW3 | 0.7286(3) | 0.6911(4) | 0.6003(3) | 5.1(1) | |
| OW4 | 0.6382(3) | 0.6202(4) | 0.4601(3) | 4.6(1) | |
| O1 | 0.6683(3) | 0.4377(4) | 0.5049(3) | 4.8(1) | |
| O2 | 0.7522(3) | 0.5011(3) | 0.6409(3) | 3.6(1) | |
| C1 | 0.6704(4) | 0.3725(5) | 0.6392(4) | 3.7(1)* | |
| C2 | 0.6385(4) | 0.3019(5) | 0.6833(4) | 4.0(1)* | |
| C3 | 0.6581(4) | 0.2837(5) | 0.7646(5) | 4.0(1)* | |
| C4 | 0.7121(4) | 0.3399(5) | 0.8023(5) | 4.1(1)* | |
| C5 | 0.7447(4) | 0.4115(5) | 0.7604(4) | 3.6(1)* | |
| C6 | 0.7231(4) | 0.4328(4) | 0.6785(4) | 3.2(1)* | |
| C7 | 0.6468(4) | 0.3803(5) | 0.5555(5) | 4.3(1)* | |
| C8 | 0.6227(5) | 0.2072(6) | 0.8110(5) | 5.2(2)* | |
| C9 | 0.8041(4) | 0.4629(5) | 0.8050(5) | 4.0(1)* | |
| N1 | 0.8382(3) | 0.5294(4) | 0.7758(4) | 3.9(1)* | |
| C10 | 0.8954(5) | 0.5807(6) | 0.8206(5) | 4.8(2)* | |
| C11 | 0.9582(5) | 0.6095(6) | 0.7667(5) | 5.0(2)* | |
| C12 | 0.9969(4) | 0.5277(5) | 0.7311(5) | 3.9(1)* | |
| C13 | 1.0486(5) | 0.4786(6) | 0.7753(5) | 5.0(2)* | |
| C14 | 1.0824(6) | 0.4053(7) | 0.7394(6) | 6.2(2)* | |
| C15 | 1.0631(5) | 0.3790(6) | 0.6610(6) | 5.7(2)* | |
| C16 | 1.0088(5) | 0.4332(6) | 0.6209(6) | 5.1(2)* | |
| N2 | 0.9766(4) | 0.5048(4) | 0.6537(4) | 4.3(1)* | |
| O3 | 0.8360(4) | 0.4308(4) | 0.5023(3) | 5.0(1) | |
| O4 | 0.7578(3) | 0.5202(3) | 0.3732(3) | 3.6(1) | |
| C17 | 0.8340(4) | 0.3857(5) | 0.3625(4) | 3.6(1)* | |
| C18 | 0.8626(4) | 0.3190(5) | 0.3127(5) | 4.3(1)* | |
| C19 | 0.8404(4) | 0.3120(6) | 0.2287(5) | 4.5(1)* | |
| C20 | 0.7893(4) | 0.3727(5) | 0.1992(5) | 4.1(1)* | |
| C21 | 0.7600(4) | 0.4442(5) | 0.2465(4) | 3.6(1)* | |
| C22 | 0.7828(4) | 0.4532(4) | 0.3304(4) | 3.3(1)* | |
| C23 | 0.8560(5) | 0.3809(6) | 0.4478(5) | 4.7(2)* | |
| C24 | 0.8718(5) | 0.2390(6) | 0.1752(6) | 5.6(2)* | |
| C25 | 0.7031(4) | 0.5000(5) | 0.2090(4) | 3.8(1)* | |
| N3 | 0.6713(3) | 0.5687(4) | 0.2401(4) | 4.0(1)* | |
| C26 | 0.6729(5) | 0.6217(6) | 0.1998(5) | 4.7(2)* | |
| C27 | 0.5511(5) | 0.6412(6) | 0.2560(5) | 5.2(2)* | |
| C28 | 0.5141(4) | 0.5580(5) | 0.2863(5) | 4.2(1)* | |
| C29 | 0.4622(5) | 0.5067(7) | 0.2372(6) | 5.6(2)* | |
| C30 | 0.4296(6) | 0.4336(7) | 0.2679(7) | 6.5(2)* | |
| C31 | 0.4481(5) | 0.4053(7) | 0.3473(6) | 5.6(5)* | |
| C32 | 0.4983(5) | 0.4570(6) | 0.3922(5) | 4.9(2)* | |
| N4 | 0.5314(4) | 0.5312(4) | 0.3635(4) | 4.3(1)* | |
| OW5 | 0.7720(8) | 0.8648(7) | 0.5481(8) | 13.6(4) | |
| OW6 | 0.5990(9) | 0.7965(8) | 0.463(1) | 15.5(6) | 0.75 |
| OW7 | 0.820(1) | 0.452(2) | 0.006(1) | 13.2(9) | 0.5 |
| OW8 | 0.702(1) | 0.922(1) | 0.429(1) | 11.9(7) | 0.5 |
| Cl1 | 0.7314(2) | 0.7850(2) | 0.2862(1) | 6.33(6) | |
| Cl2 | 0.9903(2) | 0.8329(2) | 0.5347(1) | 6.38(6) | |
| O12 | 0.9362(6) | 0.9076(7) | 0.5277(6) | 10.8(3)* | |
| O22 | 0.993(1) | 0.781(1) | 0.461(1) | 12.3(5)* | 0.5 |
| O32 | 1.0553(7) | 0.8674(9) | 0.5820(8) | 12.8(3)* | |
| O42 | 0.9640(8) | 0.764(1) | 0.5910(9) | 9.0(3)* | 0.5 |
| O52 | 1.034(2) | 0.854(2) | 0.455(2) | 11.1(7)* | 0.5 |
| O62 | 0.989(1) | 0.734(2) | 0.523(2) | 10.3(6)* | 0.5 |
| Cl3 | 0.6003(3) | 1.1086(2) | 0.5065(2) | 9.4(1) | |
| O13 | 0.5729(8) | 1.095(1) | 0.5841(8) | 13.7(4)* | |
| O23 | 0.5520(8) | 1.155(1) | 0.4515(9) | 15.1(4)* | |
| O33 | 0.6736(7) | 1.1564(8) | 0.5144(7) | 12.2(3)* | |
| O43 | 0.625(2) | 1.036(2) | 0.454(2) | 14.2(9)* | 0.5 |
| O53 | 0.591(2) | 1.009(2) | 0.497(2) | 13.8(8)* | 0.5 |

$^a$ Starred values denote atoms that were refined isotropically. Values for anisotropically refined atoms are given in the form of the isotropic equivalent displacement parameter defined as $(4/3)[a^2B(1,1) + b^2B(2,2) + c^2B(3,3) + ab(\cos\gamma)B(1,2) + ac(\cos\beta)B(1.3) + abd(\cos)B(2,3)]$. Free water molecules, $Cl2O_4$, and $Cl3O_4$ were highly disordered in the large tunnels of the structure.

**Luminescence Measurements.** The luminescence spectra of (**1**)Eu were recorded on powder samples of 77 K with the blue line at 4579 Å of a CW argon ion laser. The emission was detected with a 1-m Jarrell-Ash

**Table III.** Bond Distances and Angles around the Gd Atom in $[GdL_2(H_2O)_4](ClO_4)_2Cl\cdot 2.75H_2O$

| | | | |
|---|---|---|---|
| Gd–O1 | 2.415 (5) | Gd–OW1 | 2.377 (5) |
| Gd–O2 | 2.326 (4) | Gd–OW2 | 2.427 (5) |
| Gd–O3 | 2.421 (6) | Gd–OW3 | 2.440 (5) |
| Gd–O4 | 2.340 (4) | Gd–OW4 | 2.390 (5) |
| O2–Gd–O2 | 72.1 (2) | O1–Gd–OW3 | 116.7 (2) |
| O1–Gd–O3 | 77.8 (2) | O1–Gd–OW4 | 71.3 (2) |
| O1–Gd–O4 | 78.6 (2) | O2–Gd–O3 | 77.7 (2) |
| O1–Gd–OW1 | 141.8 (2) | O2–Gd–O4 | 141.6 (2) |
| O1–Gd–OW2 | 144.5 (2) | O2–Gd–OW1 | 80.2 (2) |
| O2–Gd–OW2 | 139.8 (2) | O4–Gd–OW2 | 76.8 (2) |
| O2–Gd–OW3 | 74.1 (2) | O4–Gd–OW3 | 143.0 (2) |
| O2–Gd–OW4 | 112.8 (2) | O4–Gd–OW4 | 79.4 (2) |
| O3–Gd–O4 | 72.2 (2) | OW1–Gd–OW2 | 71.9 (2) |
| O3–Gd–OW1 | 71.0 (2) | OW1–Gd–OW3 | 78.7 (2) |
| O3–Gd–OW2 | 117.7 (2) | OW1–Gd–OW4 | 145.5 (2) |
| O3–Gd–OW3 | 141.4 (2) | OW2–Gd–OW3 | 71.5 (2) |
| O3–Gd–OW4 | 141.4 (2) | OW2–Gd–OW4 | 79.2 (2) |
| O4–Gd–OW1 | 110.9 (2) | OW3–Gd–OW4 | 75.0 (2) |

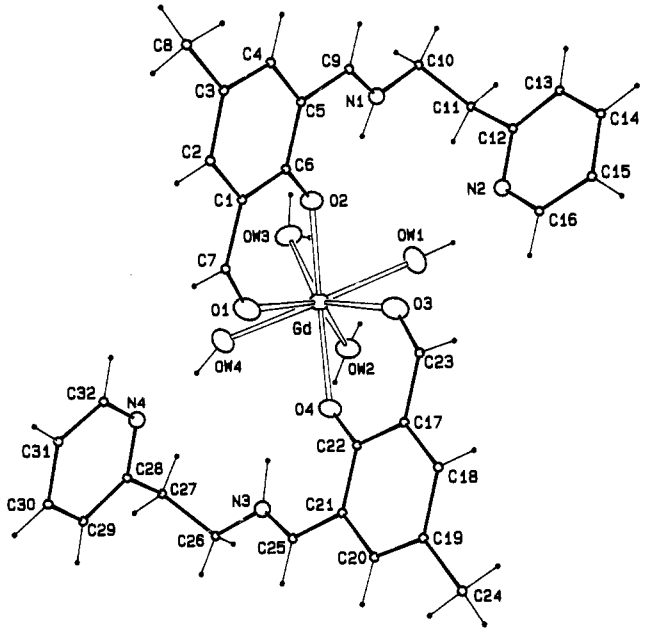


**Figure 1.** Perspective view of the cation $[GdL_2(H_2O)_4]^{3+}$.

monochromator and a Hamamatsu R374 photomultiplier. The luminescence was recorded in the wavelength range between 575 and 750 nm.

**Magnetic Measurements.** These were carried out with a Faraday-type magnetometer equipped with a helium continuous flow cryostat working in the 4.2–300 K temperature range. Diamagnetic corrections were estimated as $-500$ cm$^3$ mol$^{-1}$ for all studied compounds. For (**1**)Gd the magnetic data were measured down to 1.8 K with a SQUID magnetometer within a magnetic field of 100 Oe.

**EPR Spectra.** These with recorded at 10 K with a ER 200 Bruker spectrometer equipped with a Hall probe and a frequency meter.

## Description of the Structure of $[GdL_2(H_2O)_4](ClO_4)_2Cl\cdot 2.75H_2O$

The structure consists of $[GdL_2(H_2O)_4]^{3+}$ discrete entities, perchlorate and chloride anions in the ratio $ClO_4/Cl = 2$, and intervening water molecules. A total of 2.75 noncoordinated water molecules per Gd-containing unit were found. A view of the cationic entity is shown in Figure 1 along with the atom labeling scheme.

The gadolinium atom is coordinated by eight oxygen atoms in an almost perfect square antiprism fashion (see Figure S1). Two oxygen atoms belong to phenolato groups, two to carbonyl groups, and four to water molecules. The Gd–O bond lengths range from 2.326(4) to 2.440(5) Å. The shortest Gd–O distances involve phenolic oxygen atoms.

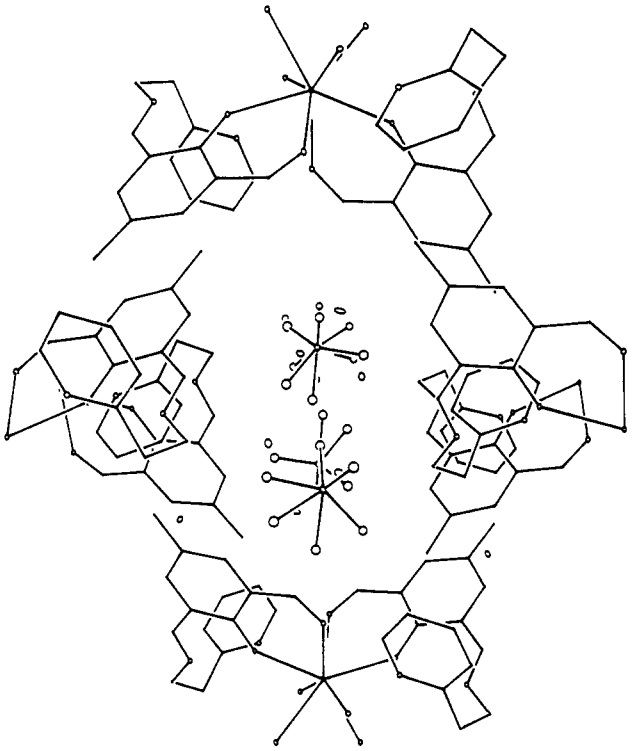

**Figure 2.** View of the tunnel formed by the $[GdL_2(H_2O)_4]^{3+}$ cations running parallel to the [100] axis.

Within each of the two ligands L the phenolic hydrogen atom has completely migrated on the nitrogen atom of the imine group, affording an iminium function, the N1–HN1 and N3–HN3 distances being equal to 1.025(6) and 1.053(6) Å, respectively. Through hydrogen bonds the four nitrogen atoms are clamped toward the close environment of the rare earth metal (N1–HN1–O2 = 114.6(4)°, N2–H2W1–OW1 = 158.3(4)°, N3–NH3–O4 = 135.8(4)° and N4–H1W4–OW4 = 155.5(2)°). The C7–O1, C9–N1, C23–O3, and C25–N3 bonds retain their double bond character. The four aromatic rings of each $[GdL_2(H_2O)_4]^{3+}$ unit are not too far from planarity, the pyridine rings being the least distorted.

The chloride anion, Cl1, is strongly hydrogen-bonded to the water molecules OW2 and OW3 (H1W2–Cl1$^i$ = 2.043(2) Å, OW2–H1W2–Cl1 = 168.7(3)°, H1W3–Cl1 = 2.156(2) Å, OW3–H1W3–Cl1$^i$ = 170.1(3)°). The perchlorate anions are also partially disordered. This disorder has not been totally resolved.

An interesting feature of this structure is the presence of tunnels running parallel to the three axes [100], [010], and [001]. The bulkiest one occurs through the [100] axis (at $y = 0, z = {}^1/_2$, and $y = {}^1/_2, z = 0$) (see Figure 2); its free aperture can be estimated as 5 × 4 Å. These tunnels are filled with the perchlorate anions and intervening water molecules. The location of these groups accounts for their high mobility, and probably contributes to the lattice cohesion. Other factors contributing to the stability of the lattice are (i) the chloride ion, which links together two cationic entities, affording thus zigzag chains parallel to the [001] direction at the level $y = 0.25$ and 0.75, and (ii) the stacking of almost parallel cycles which develop along the [110] and [$\bar{1}$10] directions. The sequence of the stacks involves the four cycles, in the order C1 to C6, C12 to N2, C17 to C22, and C28 to N4. The distances between two adjacent cycles do not exceed 3.62 Å, which allows significant $\pi$ overlaps.

## Luminescence Spectra of (1)Eu

The most striking result concerning the optical properties of (**1**)Eu is also the most easily detected. Despite the presence of four water molecules in the Eu(III) coordination sphere, (**1**)Eu shows an intense luminescence in the solid state. In most cases

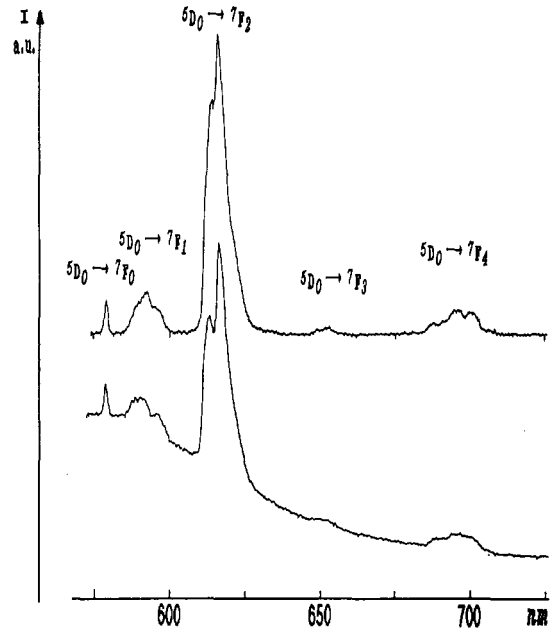


**Figure 3.** Emission spectra of (1)Eu recorded at 77 K under the 4579 Å excitation of a cw argon laser: Top, pure (1)Eu; bottom, (1)Gd doped with 3% of (1)Eu.

**Table IV.** Transition Energies (in $cm^{-1}$) for the Luminescence Spectrum of (1)Eu

| | | | |
|---|---|---|---|
| $^5D_0 \rightarrow {}^7F_0$ | 17 260 | | |
| $^5D_0 \rightarrow {}^7F_1$ | 16 975 | $^5D_0 \rightarrow {}^7F_2$ | 16 331 |
| | 16 889 | | 16 291 |
| | 16 806 | | 16 201 |

the presence of water molecules causes nonradiative decay of the luminescent metal-centered level $^5D_0$.[18-20] The reason why the luminescence is retained in our compound is not clear yet.

The excitation provided by the 4579-Å line of an argon laser roughly corresponds to the transition $^7F_0 \rightarrow {}^5D_2$. After deexcitation from $^5D_2$ to $^5D_0$ the system decays from $^5D_0$ to the $^7F_J$ low-lying states in a radiative manner.[21,22] The emission spectrum is shown in Figure 3, and the detected transitions are tabulated in Table IV. The $^5D_0 \rightarrow {}^7F_0$ transition occurs at 17 260 $cm^{-1}$. The 3-fold degeneracy of the $^7F_1$ free-ion state is totally removed. That means that, after the application of both electronic and group theory selection rules, the site symmetry of the Eu(III) ion is not higher than $C_{2v}$. However, the relatively small total splitting for that level indicates that the site symmetry is not too far from $D_{4d}$, which agrees with the structural data. The 5-fold degeneracy of the $^7F_2$ free-ion state is also expected to be totally removed. However, only three transitions are perfectly characterized. A fourth transition may be observed as a low-energy shoulder. The spectrum also shows $^5D_0 \rightarrow {}^7F_3$ and $^5D_0 \rightarrow {}^7F_4$ transitions.

Let us come back for a moment to the $^5D_0 \rightarrow {}^7F_0$ transition energy, namely 17 260 $cm^{-1}$. Horrocks et al. have proposed a correlation between this transition energy and the total charge on the ligands surrounding the Eu(III) ion.[23] In the present case this correlation indicates a −2 charge. This value is perfectly in line with the fact that when the L ligand binds to Eu(III), a hydrogen atom is displaced from the phenolic toward the imine function, affording a phenolato (-)–iminium (+) entity. Although L is neutral, the rare-earth ion sees a charge of −2 arising from the two phenolato (-) functions.

We were wondering whether the luminescence of (1)Eu was retained in solution. It is not the case in methanol. On the other hand, a surprising result was obtained in acetonitrile. A freshly prepared solution of (1)Eu in acetonitrile shows no luminescence. However, after about 1 h, the characteristic red luminescence is observed. The chemical transformation accompanying the appearance of the luminescence can be followed by absorption spectroscopy. Probably, the water molecules are replaced by acetonitrile molecules in the Eu(III) coordination sphere. It is worth mentioning that a solution of Eu(III) perchlorate in acetonitrile exhibits no luminescence.

## Magnetic Properties

For most of the trivalent rare earth ions the $^{2S+1}L_J$ free-ion ground state is well separated in energy from the first excited state, such that only this ground state is thermally populated at room temperature and below. In the free-ion approximation the molar magnetic susceptibility for a mononuclear species is then given by[14,24,25]

$$\chi(J) = \frac{Ng_J^2\beta^2J(J+1)}{3kT} + \frac{2N\beta^2(g_J-1)(g_J-2)}{3\lambda} \quad (1)$$

where $T$ is the temperature and $g_j$ is the Zeeman factor

$$g_J = {}^3/_2 + [S(S+1) - L(L+1)]/2J(J+1) \quad (2)$$

$L$ being the orbital quantum number. The second term in the right-hand side of eq 1 is a temperature-independent contribution arising from the coupling between ground and excited states through the Zeeman perturbation; $\lambda$ is the spin–orbit coupling parameter. For rare earth mononuclear compounds the $\chi_M T$ versus $T$ plot in general deviates somewhat from what is predicted from eq 1. This deviation may be due to two effects, namely (i) the crystal field, which partially removes the $2J + 1$ degeneracy of the ground state in zero field, and (ii) the thermal population of free-ion excited states, which happens with Eu(III) and Sm(III). To get new insights on the magnetic properties of rare-earth mononuclear species, we investigated the temperature dependences of the magnetic susceptibility of (1)M compounds with M = Gd, Nd, Eu, and Sm.

**(1)Gd.** The $^8S_{7/2}$ ground state is located at some $10^4$ $cm^{-1}$ below the first excited state, and is not perturbed by crystal field effects. The Zeemann factor $g_J$ is equal to 2, and the TIP term appearing on the right-hand side of eq 1 is expected to be negligible. It turns out that the magnetic susceptibility should obey the Curie law $\chi_M T = 21N\beta^2/k$. The experimental data are in line with this; $\chi_M T$ is constant and equal to 7.70 ± 0.05 $cm^3$ K $mol^{-1}$ down to 4.2 K. As $T$ is lowered further below 4.2 K, $\chi_M T$ decreases very slightly, and reaches 7.5 $cm^3$ K $mol^{-1}$ at 1.8 K, which is probably due to a very small zero-field splitting within the $^8S_{7/2}$ state. The presence of this zero-field splitting is clearly demonstrated by the EPR spectrum at 10 K shown in Figure 4. This spectrum may be interpreted from the fine structure Hamiltonian

$$H_{FS} = DS_z^2 \quad (3)$$

in which the zero-field splitting is assumed to be axial, with the

(18) Albin, M.; Goldstone, A. C.; Withers, A. S.; Horrocks, W. D., Jr. *Inorg. Chem.* **1983**, *22*, 3182.
(19) Hazenkamp, M. F.; Blasse, G.; Sabbatini, N.; Ungaro, R. *Inorg. Chim. Acta* **1990**, *12*, 93.
(20) Prodi, L.; Maestri, M.; Ziessel, R.; Balzani, V. *Inorg. Chem.* **1991**, *30*, 3798.
(21) Antic-Fidancev, E.; Hölsä, J.; Lemaitre-Blaise, M.; Porcher, P. *J. Phys.: Condens. Matter* **1991**, *3*, 6829.
(22) Cascales, C.; Antic-Fidancev, E.; Lemaitre-Blaise, M.; Porcher, P. *J. Phys.: Condens. Matter* **1992**, *4*, 2721.
(23) Albin, M.; Horrocks, W. D. *Inorg. Chem.* **1985**, *24*, 895.
(24) Casey, A. P. In *Theory and Applications of Molecular Paramagnetism*; Boudreaux, E. A., Mulay, L. N. Eds.; John Wiley: New York, 1976; p 27.
(25) Kahn, O. *Molecular Magnesism*; VCH: New York, in press.

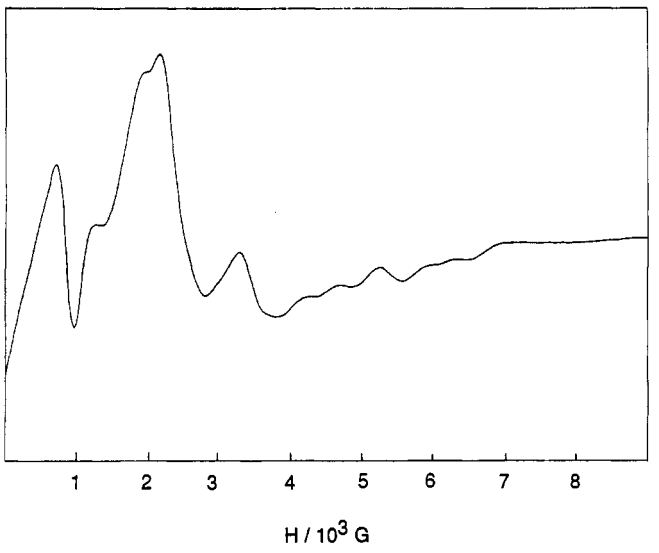


**Figure 4.** X-Band powder EPR spectrum at 10 K of (**1**)Gd.

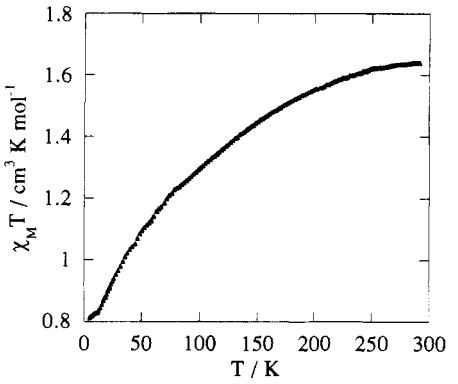


**Figure 5.** $\chi_M T$ versus $T$ plot for (**1**)Nd.

parameter $D$. Equation 3 leads to the resonant fields

$$H_1 = h\nu/g\beta$$

$$H_{2,3} = (h\nu \pm 2D)/g\beta$$

$$H_{4,5} = (h\nu \pm 4D)/g\beta$$

$$H_{6,7} = (h\nu \pm 6D)/g\beta \quad (4)$$

The spectrum actually exhibits the seven expected transitions around 820, 1670, 2520, 3370, 4220, 5070 and 5920 G, which correspond to $g \approx 1.99$ and $|D| = 4.0 \times 10^{-2}$ cm$^{-1}$. The agreement between what the axial model predicts and the experimental spectrum may seem to be surprising at the first view. However, it is in line with the fact that the structure is close to a square antiprism, with $D_{4d}$ symmetry. It may be worth reminding that the zero-field splitting within the $^8S_{7/2}$ state arises from the coupling of this state with $^6P_{7/2}$ through the spin-orbit coupling.

**(1)Nd.** The free-ion ground state of Nd(III) is $^4I_{9/2}$. The first excited state, $^4I_{11/2}$, is located at some 2000 cm$^{-1}$ above, such that it is fully depopulated, even at room temperature. The Zeeman factor, $g_J$, is equal to 8/11. It turns out that eq 1 leads to $\chi_M T$ = 1.64 cm$^3$ K mol$^{-1}$.

The $\chi_M T$ versus $T$ curve for (**1**)Nd is shown in Figure 5. At room temperature $\chi_M T$ is equal to 1.64 cm$^3$ K mol$^{-1}$, which is exactly what eq 1 predicts. However, the magnetic behavior does not follow the Curie law. As $T$ is lowered, $\chi_M T$ decreases more and more rapidly, and finally reaches a low-temperature limit of 0.80 cm$^3$ K mol$^{-1}$. In the $100 < T/K < 300$ range, the magnetic data obey the Curie–Weiss law $\chi_M/\text{cm}^3\,\text{mol}^{-1} = 1.937/(T/K - 50.5)$ (see Figure S2). The Weiss constant $\Theta = -50.5$ K agrees with previously reported values.[14]

The important deviation of the magnetic susceptibility with respect to the Curie law is due to the crystal field which splits the $^4I_{9/2}$ free-ion ground state into five Kramers doublets. These doublets are almost equally populated at 300 K, such that $\chi_M T$ is equal to the value calculated in the free-ion approximation (eq 1). As the temperature decreases, the Kramers doublets of higher energy are progressively depopulated. When only the lowest Kramers doublet is populated, $\chi_M T$ approaches a limit of 0.80 cm$^3$ K mol$^{-1}$. A theoretical simulation of the magnetic properties would be possible in principle. This would require the diagonalization of spin–orbit coupling, crystal field, and Zeeman perturbation using all the kets associated with the $^{2S+1}\Gamma_J$ free-ion states arising from the 4f$^3$ configuration as a basis set. Such an approach is clearly overparametrized, unless the crystal field parameters may be determined separately from the optical properties.

**(1)Eu.** The $^7$F ground term is split by the spin-orbit coupling into seven states, $^7F_J$, with $J$ taking integer values from 0 to 6, and the energies of the states are

$$E(J) = \lambda J(J+1)/2 \quad (5)$$

where the energy of the $^7F_0$ ground state is taken as the origin. Since $\lambda$ is small enough for the first excited states to be thermally populated, the magnetic susceptibility may be expressed as

$$\chi_M = \frac{\sum_{J=0}^{6}(2J+1)\chi(J)\exp[-\lambda J(J+1)/2kT]}{\sum_{J=0}^{6}(2J+1)\exp[-\lambda J(J+1)/2kT]} \quad (6)$$

where $\chi(J)$ is given by eq 1. In the present case all of the $g_J$ factors are equal to 3/2, except $g_0$ which is equal to[24,25] $2 + L (=2 + S) = 5$. It follows that $\chi_M$ can be expanded as

$$\chi_M = (N\beta^2/3kTx)[24 + (27x/2 - 3/2)e^{-x} + (135x/2 - 5/2)e^{-3x} + (189x - 7/2)e^{-6x} + (405x - 9/2)e^{-10x} + (1485x/2 - 11/2)e^{-15}x + (2457x/2 - 13/2)e^{-21x}]/[1 + 3e^{-x} + 5e^{-3x} + 7e^{-6x} + 9e^{-10x} + 11e^{-15x} + 13e^{-21x}] \quad (7)$$

with

$$x = \lambda/kT \quad (8)$$

The high-temperature limit $(\chi T)_{HT}$, for $kT \gg \lambda$, is obtained by assuming that the magnetic susceptibility of the $^7$F term is the sum of an orbital contribution and a spin contribution, according to

$$(\chi_M T)_{HT} = (N\beta^2/3k)[g_L^2 L(L+1) + g_S^2 S(S+1)] \quad (9)$$

with $g_L = 1$, and $g_S = 2$. This high-temperature limit would then be equal to $12N\beta^2/k$, namely 4.50 cm$^3$ K mol$^{-1}$. Actually this limit cannot be reached. Indeed, owing to the value of $\lambda$, only the first three low-lying states with the energies 0, $\lambda$, and $3\lambda$ can be significantly populated. As for the low-temperature limit of $\chi T$, it is zero because the $^7F_0$ ground state is nonmagnetic. The low-temperature limit $(\chi_M)_{LT}$ of the magnetic susceptibility is finite and nonzero owing to the term $\chi(0)$ arising from the coupling between the $^7F_0$ and $^7F_1$ states through the Zeeman perturbation.

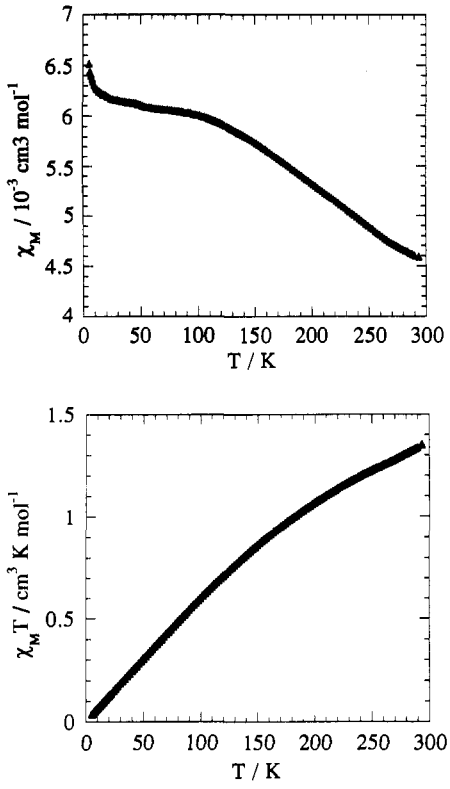


**Figure 6.** $\chi_M$ (top) and $\chi_M T$ versus $T$ (bottom) plots for (1)Eu.

$(\chi_M)_{LT}$ is simply related to $\lambda$ through[26-28]

$$(\chi_M)_{LT} = 8N\beta^2/\lambda = (2.086 \times 10^{-3})/(\lambda \text{ in cm}^{-1}) \quad (10)$$

The $\chi_M$ and $\chi_M T$ versus $T$ plots are shown in Figure 6. As T is lowered, $\chi_M$ smoothly increases and then tends to a plateau. At very low temperatures $\chi_M$ increases again as T is lowered further due to the unavoidable presence of a few parts per million of a rare earth metal ion with a paramagnetic ground state in the sample. As expected $\chi_M$T continuously decreases and tends to a value very close to zero as $T$ approaches absolute zero. Below ca. 50 K, $\chi_M T$ varies rigorously linearly versus $T$, with the slope $(\chi_M)_{LT} = 5.99 \times 10^{-3}$ cm$^3$ mol$^{-1}$. A least-squares fitting of the $\chi_M T$ versus $T$ curve leads to $\lambda = 362$ cm$^{-1}$. The agreement factor defined as $\sum[(\chi_M T)^{calcd} - (\chi_M T)^{obs}]^2/\sum[(\chi_M T)^{obs}]^2$ is then equal to $7 \times 10^{-4}$, which corresponds to a satisfying but not perfect theory–experiment agreement. $\lambda$ can be also determined directly from eq 10, which leads to $\lambda = 348$ cm$^{-1}$. At this stage, it is interesting to compare the $\lambda$ value deduced from the magnetic data in the free-ion approximation to the value deduced from the spectroscopic data. $\lambda$ is the energy gap between the $^7F_1$ and $^7F_0$ free-ion states. When the three components arising from $^7F_1$ are averaged, $\lambda$ is found equal to 370 cm$^{-1}$. The agreement between spectroscopic and magnetic data is quite good.

It is worth mentioning that in the approximation where the crystal field is weak, $(\chi_M)_{LT}$ may be related to the energies in cm$^{-1}$ $E_i$, $i$ = 1–3, of the three components arising from $^7F_1$ through[26,27]

$$(\chi_M)_{LT} = 0.6953(1/E_1 + 1/E_2 + 1/E_3) \quad (11)$$

the energy origin being the $^7F_0$ ground state. For $E_1 = E_2 = E_3$, eqs 10 and 11 are evidently equivalent. Equation 11 together with the $E_i$ energies deduced from Table IV leads to $(\chi_M)_{LT} = 5.85 \times 10^{-3}$ cm$^3$ mol$^{-1}$, which compares fairly well with the experimental value of $5.99 \times 10^{-3}$ cm$^3$ mol$^{-1}$.

(26) Ofelt, G. S. *J. Chem. Phys.* **1963**, *38*, 2171.
(27) Huang, J.; Loriers, J.; Porcher, P.; Teste de Sagey, G.; Caro, P. *J. Chem. Phys.* **1984**, *80*, 6204.
(28) Caro, P.; Porcher, P. *J. Magn. Magn. Mater.* **1986**, *58*, 61.

**(1)Sm.** The $^6H$ ground term for Sm(III) is split by spin–orbit coupling into six levels. The energies, $E(J)$, increase from $^6H_{5/2}$ to $^6H_{15/2}$. These energies are

$$E(J) = \lambda[J(J+1) - {}^{35}/_4]/2 \quad (12)$$

The energy of the ground state is again taken as the origin. The spin–orbit coupling parameter is of the order of 200 cm$^{-1}$, such that the first excited state $^6H_{7/2}$ can be populated at room temperature and above. The expression of the magnetic susceptibility taking into account the six states arising from $^6H$ is

$$\chi_M = \frac{\sum_{J=5/2}^{15/2}(2J+1)\chi(J)\exp[-E(J)/kT]}{\sum_{J=5/2}^{15/2}(2J+1)\exp[-E(J)/kT]} \quad (13)$$

$\chi(J)$ being given by eq 1 and $E(J)$ by eq 12. $\chi_M$ may be expanded as

$$\chi_M = (N\beta^2/3kTx)[a_1x + b_1 + (a_2x + b_2)e^{-7x/2} + (a_3x + b_3)e^{-8x} + (a_4x + b_4)e^{-27x/2} + (a_5x + b_5)e^{-20x} + (a_6x + b_6)e^{-55x/2}]/[3 + 4e^{-7x/2} + 5e^{-8x} + 6e^{-27x/2} + 7e^{-20x} + 8e^{-55x/2}] \quad (14)$$

with

$$a_1 = 2.143 \quad b_1 = 7.347$$
$$a_2 = 42.92 \quad b_2 = 1.641$$
$$a_3 = 283.7 \quad b_3 = -0.6571$$
$$a_4 = 620.6 \quad b_4 = -1.9400$$
$$a_5 = 1122 \quad b_5 = -2.835$$
$$a_6 = 1813 \quad b_6 = -3.556 \quad (15)$$

and $x$ defined as in eq 8. As was the case for Eu(III), $E(J)$ and $\chi(J)T$ decrease with $J$. Therefore $\chi_M T$ decreases as $T$ decreases and tends to the value 0.89 cm$^3$ K mol$^{-1}$ as $T$ approaches absolute zero. This magnetic behavior is rather unusual in the sense that eq 13 predicts that the $\chi_M$ versus $T$ curve should exhibit a rounded minimum for a $T$ value defined by $kT/\lambda = 0.956$. The experimental $\chi_M$ and $\chi_M T$ versus $T$ plots are shown in Figure 7. $\chi_M$ does not show the minimum predicted by eq 13 but is almost constant around room temperature. The temperature dependence of $\chi_M T$ is nearly linear over the whole temperature range. When $T$ approaches absolute zero, $\chi_M T$ tends to the low-temperature limit $(\chi_M T)_{LT} = 0.89$ cm$^3$ K mol$^{-1}$ predicted by the theory. The least-squares fitting of both the $\chi_M$ and $\chi_M T$ versus $T$ curves leads to $\lambda = 193$ cm$^{-1}$. The agreement factor defined as in the Eu(III) case is then equal to $2.2 \times 10^{-5}$, which corresponds to an excellent theory–experiment agreement.

## Conclusion

One of the goals of this work was to see to what extent the free-ion approximation is appropriate to interpret the magnetic properties of rare earth metal mononuclear species. For that we focused on four compounds, with Gd(III), Nd(III), Eu(III), and Sm(III).

The Gd(III) case is obviously very simple. The magnetic susceptibility follows the Curie law, except in the very low-temperature range where a zero-field splitting within the $S = {}^7/_2$

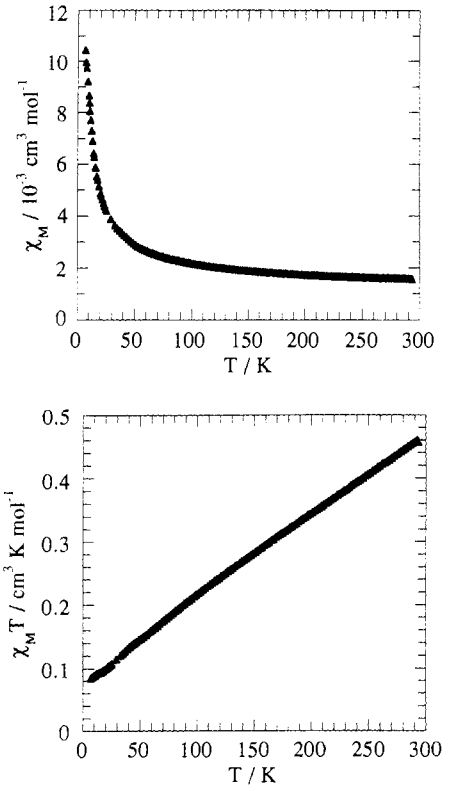


**Figure 7.** $\chi_M$ (top) and $\chi_M T$ versus $T$ (bottom) plots for (**1**)Sm.

state, characterized by an axial parameter $|D| = 4.0 \times 10^{-2}$ cm$^{-1}$, influences the magnetic behavior.

For the Nd(III) compound also, only the free-ion ground state, $^4I_{9/2}$, is thermally populated up to 300 K. However, this state is split into five Kramers doublets by the crystal field. At room temperature those doublets are equally populated, such that the magnetic susceptibility is equal to what the free-ion approximation predicts. On the other hand, as the temperature decreases, the Kramers doublets are successively depopulated, and the magnetic behavior significantly deviates from the Curie law predicted by the free-ion approximation. At 4.2 K, when only the ground Kramers doublet is thermally populated, the $\chi_M T$ value is twice as small as that at room temperature. It is worth mentioning here that in his book Carlin wrote "the susceptibility (for a Nd(III) compound) follows the curie law up to 100 K, which is consistent with only one doublet being populated until this temperature is reached".[15] Our results do not agree with this assertion. In (**1**)Ne, the energy gap between ground and first excited Kramers doublets is only of a few wavenumbers. This disagreement confirms, if it were still necessary, that the magnetic properties of rare earth metal molecular compounds deserve to be investigated in a thorough fashion. This is even true for very isolated mononuclear species, in which there is no detectable interaction between magnetic centers.

For both Eu(III) and Sm(III) several free-ion states may be populated at room temperature, which leads to magnetic properties deviating from the Curie law, even in the free-ion approximation. We used this free-ion approximation to fit the magnetic data and found an agreement with is fairly good for (**1**)Eu and excellent for (**1**)Sm. This agreement does not mean that the free-ion states remain unperturbed by the crystal field. The luminescence spectra of (**1**)Eu clearly show the splitting of the $^7F_J$ ($J \neq 0$) states. For (**1**)Eu, only the excited states are split by the crystal field, such that the free-ion approximation might be expected to be valid. For (**1**)Sm, even the $^6H_{5/2}$ ground state is split into three Kramers doublets, and the validity of the free-ion approximation is more surprising.

Let us come back for a moment to (**1**)Eu. The magnetic behavior is characterized by the low-temperature plateau $(\chi_M)_{LT}$ arising from the coupling between $^7F_0$ and $^7F_1$ states through the Zeeman perturbation. The $(\chi_M)_{LT}$ value directly depends on the energy gap between those two states. In this respect, it is quite satisfying that optical and magnetic properties agree with each other.

This paper was devoted to the structure and the physical properties of some of the (**1**)M compounds, M being a trivalent rare earth metal. The following paper will describe the unique chemistry associated with those compounds.[29]

**Acknowledgment.** M.A. would like to express his gratitude to the French Ministery for Research and Technology, which financially supported his stay in France.

**Supplementary Material Available:** Tables giving crystal data and details of the structure determination, hydrogen atom parameters, bond lengths and angles within the ligand L, and hydrogen bonds and van der Waals interactions and figures showing a view of the inner coordination polyhedron of the gadolinium atom in $[GdL_2(H_2O)_4]^{3+}$ (Figure S1) and the $\chi_M^{-1}$ versus $T$ plot for (**1**)Nd (Figure S2) (6 pages). Ordering information is given on any current masthead page.

(29) Andruh, M.; Kahn, O.; Sainton, J.; Dromzee, Y.; Jeannin, S. *Inorg. Chem.*, following paper in this issue.